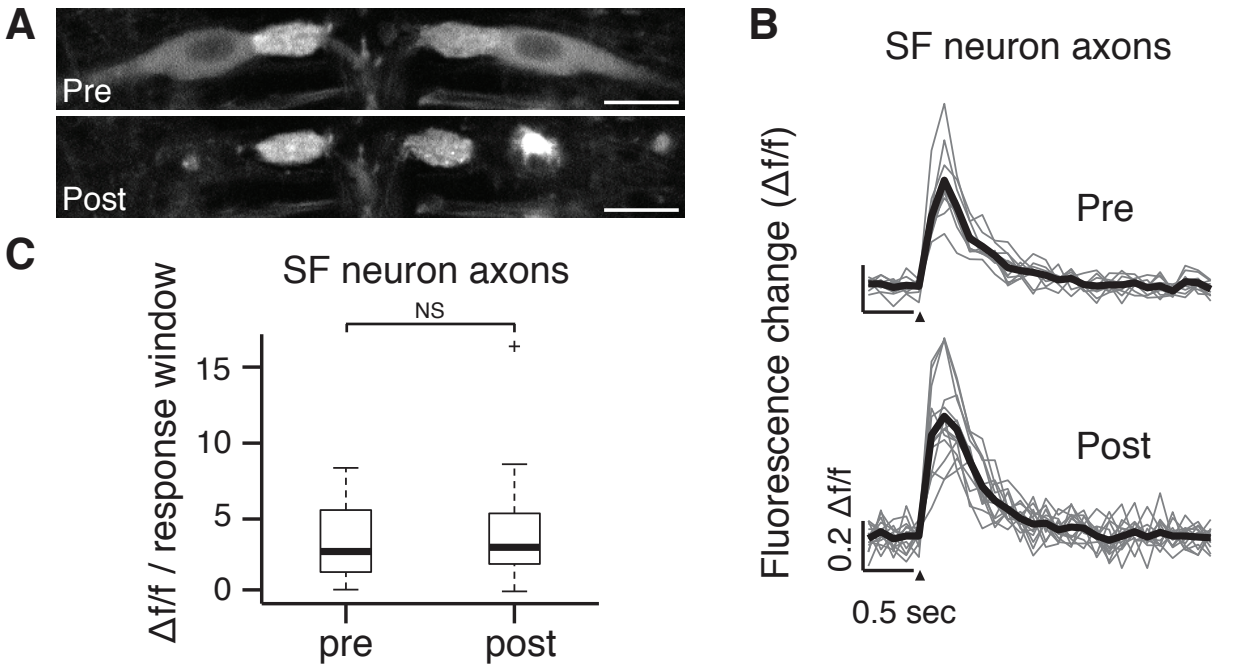


**Figure S1, related to Figure 1. Spiral fiber neuron axons continue to respond to taps after M-cell ablations.**

(A) Two-photon image showing M-cells and spiral fiber neuron axon terminals labeled with GCaMP-HS at the axon cap before (top image) and after (bottom image) bilateral ablation of the M-cells. Bright spots in the bottom image correspond to cell debris. Scale bar: 20 μm. Pictures are oriented rostral up.

(B) Representative traces of the change in spiral fiber (SF) neuron axon fluorescence at the M-cell axon cap in response to taps. Top plot: before, bottom plot: after bilateral ablation of the M-cells. Grey traces are individual trials, the black trace is the mean. Stimulus delivery is indicated by an arrowhead.

(C) Population fluorescence change of spiral fiber (SF) neuron axons in response to taps before (left) and after (right) ablation of the M-cells (n = 10 axon caps, y-axis is the mean fluorescence change over a 1.5 sec response window in trials where the axon cap responded). Horizontal line is the median, box edges are the 25th and 75th percentiles, whiskers extend to the most extreme data points not considered outliers and crosses are outliers. Pre and post are not significantly different (NS, p = 1, Wilcoxon signed rank sum test).

Abbreviation: SF: spiral fiber.

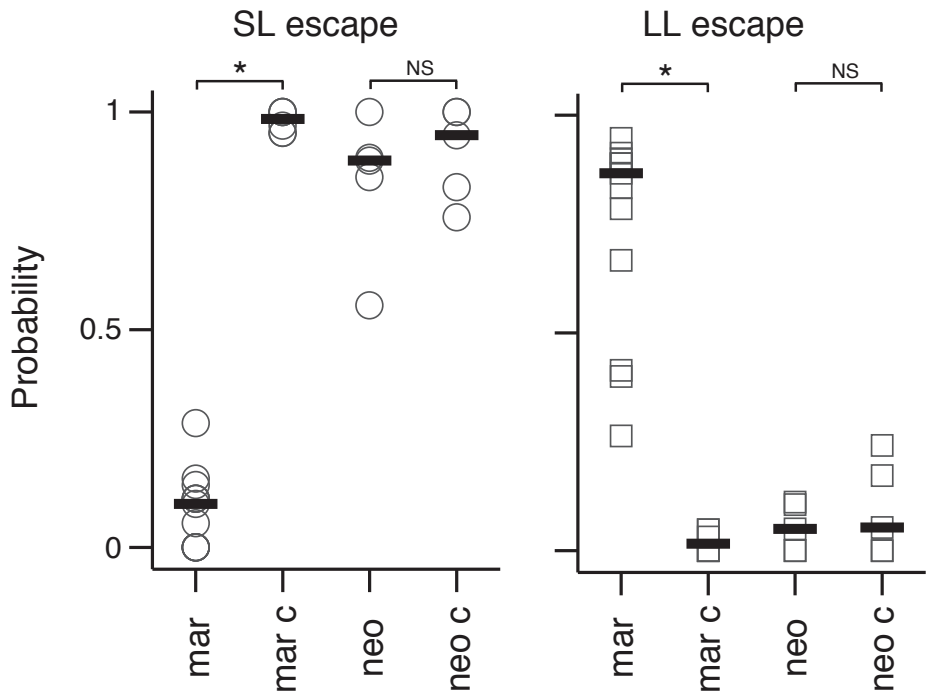


**Figure S2, related to Figure 2. Short-latency escapes in response to taps are mediated by the inner ear.**

Probability of generating escapes in response to taps in the tail-free behavioral apparatus. Fish tested are homozygote *mariner* mutant fish lacking mechanosensory transduction in hair cells (mar, n = 13) and wild-type or heterozygote siblings (mar c, n = 6); neomycin-treated fish with ablated lateral lines (neo, n = 5) and control siblings (neo c, n = 5). Left panel: short-latency (SL) escapes. Right panel: long-latency (LL) escapes. Mariner mutants are significantly different from their controls ($p = 7.4*10^{-5}$ and $7.4*10^{-5}$ for SL and LL escapes respectively) whereas neomycin treated fish and their controls are not ($p = 0.69$ and 0.65). * denotes $p < 0.05$ by Wilcoxon rank sum test.

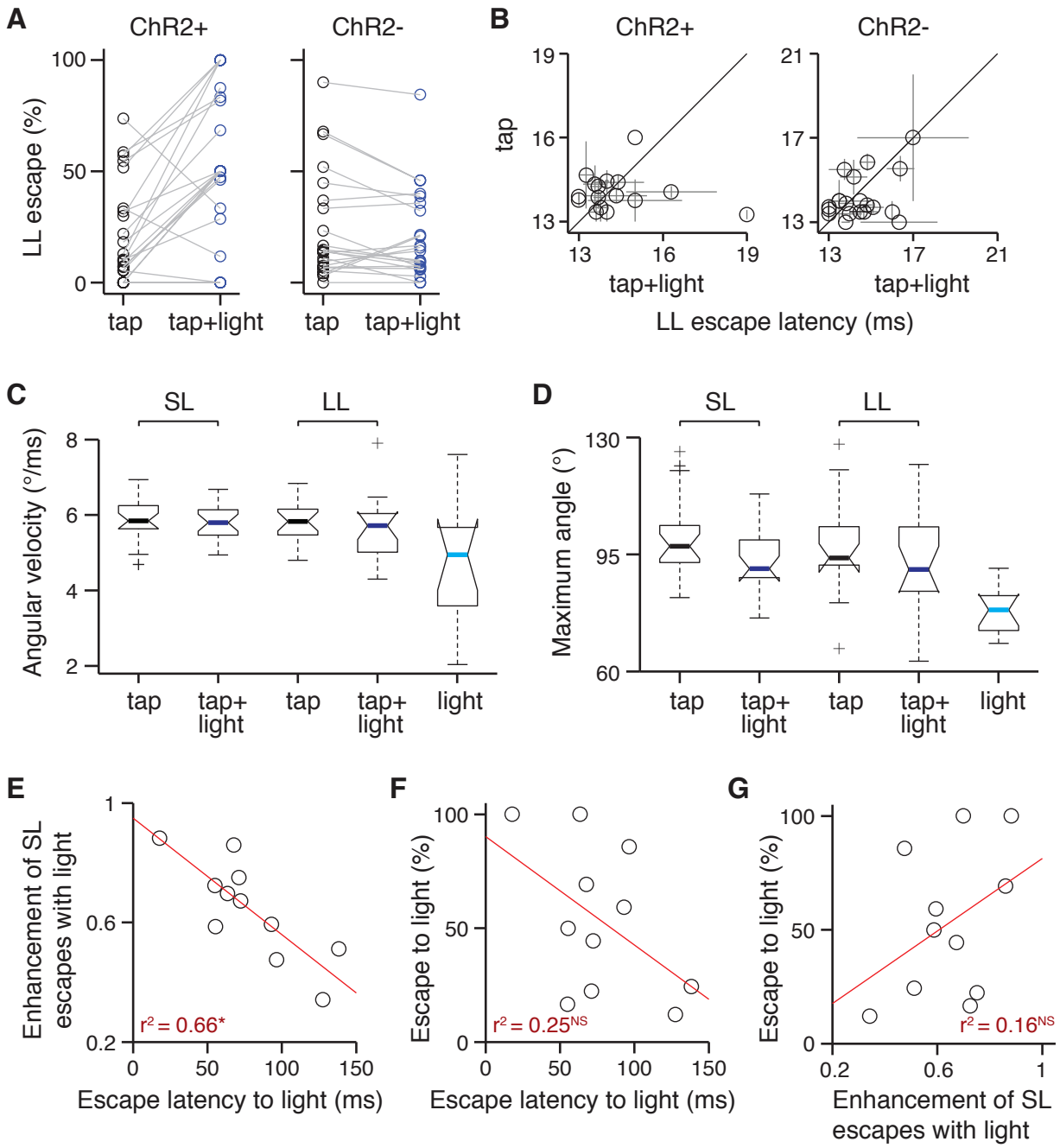


**Figure S3, related to Figure 4. Characteristics of escapes with optogenetic activation of spiral fiber neurons.**

(A) % Long-latency (LL) escapes for individual fish in response to taps alone (black circles) and taps paired with blue light (blue circles). Left panel: ChR2+ fish (n = 22, 23% ± 4.9% tap, 54% ± 7.1% tap + light, mean ± SEM, corresponding to a 2.4 fold enhancement of LL escapes with blue light, $p = 6.8*10^{-4}$). Part of this enhancement could be due to the blue light alone eliciting

escapes. Right panel: ChR2- controls (n = 22, 25% ± 5.3% tap, 21% ± 4.4% tap + light, p = 0.12, Wilcoxon signed rank test).
(B) LL escape latency in ms in response to taps (y-axis) or taps paired with blue light (x-axis). Left panel: ChR2+ fish (n = 22, 14.4 ms ± 0.41 ms tap, 14.3 ms ± 0.30 ms tap + light, mean ± SEM, p = 0.57). Right panel: ChR2- fish (n = 22, 14.1 ms ± 0.23 ms tap, 14.5 ms ± 0.25 ms tap + light, p = 0.27).
(C) Mean angular velocity of the initial C-bend in SL or LL escapes in response to taps, taps paired with blue light in ChR2+ larvae (n = 22), or blue light alone in ChR2+ larvae whose response probability to light alone exceeded 10% (n = 11). Horizontal lines are the medians across fish, box edges are the 25th and 75th percentiles, whiskers extend to the most extreme data points not considered outliers, box plots whose notches do not overlap have different medians at the 5% significance level, and crosses are outliers. The light condition is significantly different from the other 4 conditions. Other comparisons are not significant (multiple comparisons test after ANOVA, $\alpha = 0.05$).
(D) Mean maximum angle of the initial C-bend in SL or LL escapes in response to taps, taps paired with blue light in ChR2+ larvae (n = 22), or blue light alone in ChR2+ larvae whose response probability to light alone exceeded 10% (n = 11). The light condition is significantly different from the other 4 conditions. Other comparisons are not significant.
(E–G) Correlation between escape latency in response to blue light, enhancement in the probability of SL escapes when taps are paired with blue light (probability of SL escapes to tap+light - probability of SL escapes to tap), and probability of escapes to blue light. ChR2+ larvae whose response probability to light alone exceeded 10% are represented as circles (11/22 tested). $r^2$ values represent the goodness of fit from linear regression (red line). * denotes $p < 0.05$; NS: $p > 0.05$ comparing F-statistics and constant model.
Abbreviations: ChR2: channelrhodopsin 2; LS: short-latency; LL: long-latency.

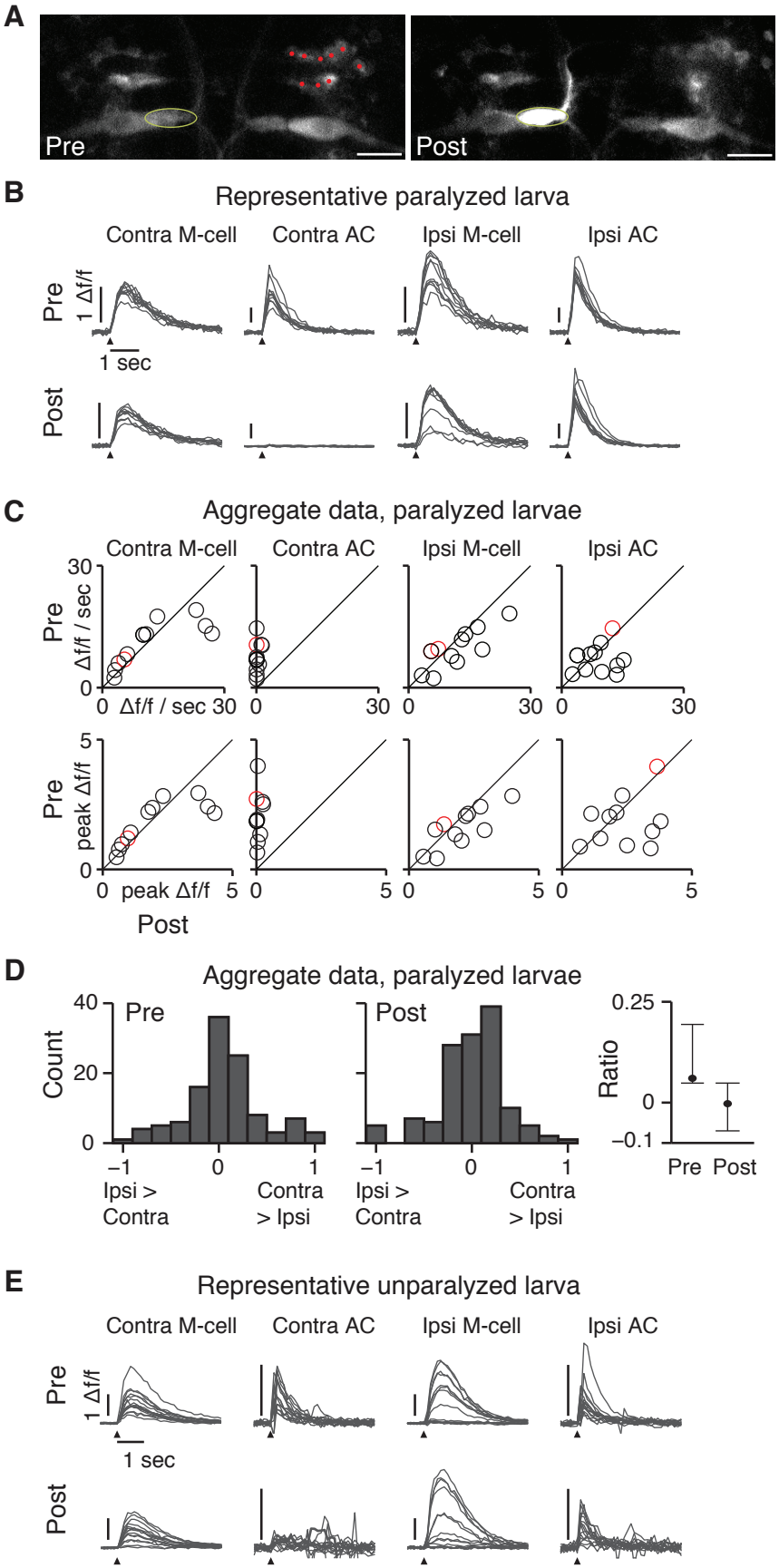
A
Pre
Post
B
Representative paralyzed larva
Contra M-cell
Contra AC
Ipsi M-cell
Ipsi AC
Pre
1 Δf/f
1 sec
Post
C
Aggregate data, paralyzed larvae
Contra M-cell
Contra AC
Ipsi M-cell
Ipsi AC
Pre
Δf/f / sec
30
0
0 Δf/f / sec 30
peak Δf/f
5
0 peak Δf/f 5
Post
D
Aggregate data, paralyzed larvae
Pre
Post
Count
40
20
0
−1
0
1
Ipsi > Contra
Contra > Ipsi
Ratio
0.25
0
−0.1
Pre Post
E
Representative unparalyzed larva
Contra M-cell
Contra AC
Ipsi M-cell
Ipsi AC
Pre
1 Δf/f
1 sec
Post

**Figure S4, related to Discussion. Spiral fiber neuron ablations do not change somatic M-cell calcium dynamics in response to taps.**

(A) Projection of two-photon image stack showing M-cells and spiral fiber neurons in *Tg(-6.7FRhcrtR:gal4VP16)* ; *Et(fos:Gal4-VP16)s1181t* ; *UAS:GCaMP5* (projection). Top: before ablation of spiral fiber neurons on the right (red dots). Bottom: immediately after ablations. The left axon cap corresponding to spiral fiber neuron axons (green oval) fluoresces strongly due to calcium release upon ablations. Scale bar: 20 μm. Pictures are oriented rostral up.

(B) Change in fluorescence (Δf/f) in response to taps (arrowheads) before and after unilateral spiral fiber neuron ablations for one representative fish paralyzed with alpha-bungarotoxin and embedded in agarose. Contra M-cell: M-cell located contralateral to the ablated spiral fiber neuron somata; Contra AC: contralateral axon cap corresponding to axon terminals of the ablated spiral fiber neurons; Ipsi M-cell: ipsilateral M-cell with preserved spiral fiber neuron input; Ipsi AC: axon cap corresponding to axon terminals of the intact spiral fiber neurons. The mean across trials is plotted in black and individual trials in grey. Top panels: before unilateral spiral fiber neuron ablations; bottom panels: after spiral fiber neuron ablations. Stimulus delivery is indicated by an arrowhead.

(C) Mean response amplitude in individual larvae (circles), before and after unilateral spiral fiber neuron ablations. First row: values represent the mean Δf/f / sec, which was computed over a 1.5 sec response window across trials with a non-zero Δf/f. The median difference pre versus post was statistically significant only in the contralateral axon cap (Contra M-cell, $p = 0.90$; Contra AC, $p = 9.8*10^{-4}$; Ipsi M-cell, $p = 0.067$; Ipsi AC, $p = 0.46$, Wilcoxon signed rank test, n = 11 fish). Second row: values represent the mean peak Δf/f across all trials. The median difference pre versus post was statistically significant only in the contralateral axon cap (Contra M-cell, p = 0.90; Contra AC, p = 9.8*10-4; Ipsi M-cell, p = 0.083; Ipsi AC, p = 0.46). The identity line is in black and the red circle represents the fish exemplified in B.

(D) Histograms showing the distribution of activity ratios between the ipsilateral and the contralateral M-cell before and after unilateral spiral fiber neuron ablations (ratio of response amplitudes normalized from -1 to 1: (contra - ipsi) / (contra + ipsi), Δf/f / sec, discarding trials in which both M-cell responses were flat, n = 130 trials pre and 139 trials post, across 11 larvae). Third panel: Histogram mean and 95% confidence interval (0.12, [0.010, 0.22], pre; 0, [-0.11, 0.11], post; p = 0.18, Wilcoxon rank sum test).

(E) Same as in B. except data is from a representative larva that was not paralyzed. Responses of the M-cells are graded and not affected by spiral fiber neuron ablations, similarly to responses in paralyzed fish.

Abbreviations: Contra: contralateral; Ipsi: ipsilateral; AC: spiral fiber neuron axon terminals at the axon cap.

## SUPPLEMENTAL RESULTS AND DISCUSSION ASSOCIATED WITH FIGURE S4

### Results. Spiral fiber neuron ablations do not change calcium dynamics in the M-cell soma in response to taps.

In response to auditory/vibrational stimuli, the M-cell receives two spatially segregated inputs, sensory afferents synapsing onto its dendrites, and spiral fiber neurons projecting to its axon hillock. An interesting question is where on the subcellular structure of the M-cell these two pathways converge. To test the effect of spiral fiber neuron input onto the M-cell, we analyzed M-cell calcium dynamics in response to taps before and after unilateral ablations of spiral fiber neurons (Figure S4A). Calcium signals could only be observed in the M-cell soma and not at the axon or axon hillock when spiral fiber neurons were not labeled. Therefore, unilateral spiral fiber neuron ablations allowed us to compare the M-cell soma lacking spiral fiber neuron projections with the other M-cell that retained spiral fiber neuron input, in the same animal.

We found that after unilateral spiral fiber neuron ablation, contralateral axon terminals failed to respond to taps, confirming the death of their associated somata (Figures S4B and S4C). M-cell and spiral fiber neuron axons ipsilateral to the ablated spiral fiber neuron somata continued to respond to stimuli with comparable fluorescence changes ($p > 0.05$, Wilcoxon signed rank test, Figures S4B and S4C). Contralateral M-cells that had lost spiral fiber neuron input also continued to respond to stimuli, and response amplitudes were comparable to the levels before spiral fiber neuron ablations ($p > 0.05$, Figure S4B). Comparing the relative amplitude of responses in the contralateral vs. ipsilateral M-cell, we found that this ratio did not change significantly after spiral fiber neuron ablations (Figure S4D). Our results were similar whether or not the larvae were paralyzed using alpha-bungarotoxin (Figure S4E). These results indicate that dendritic inputs are responsible for the bulk of calcium signals in the M-cell soma.

### Discussion. Direct and feedforward excitatory inputs are integrated at the M-cell axon hillock.

The combined anatomical ([S1, S2]; Figure 1), electrophysiological ([S2, S3]), ablation (Figures 2 and 3), optogenetic (Figure 4), and calcium imaging (Figure S4) data support a model wherein spiral fiber neuron and afferent inputs are integrated at the level of the M-cell axon hillock. Others have found that large amplitude calcium activity in the M-cell is correlated with short-latency escapes, and similar to calcium activity elicited by antidromic action potentials [S4]. Our

results suggest that without spiral fiber neuron input, the M-cell's ability to fire is compromised. One might ask, then, why the loss of spiral fiber neuron input did not decrease calcium levels in the M-cell soma. Differences between our study and published reports may explain this apparent inconsistency. First, while others mainly observe all or none calcium events in the M-cells that are thought to indicate firing events [S4-S7], our recordings show graded responses (Figures S4B, S4D and S4E). This difference may be due to the type of calcium indicator or the type of stimulus used. Second, studies using unilateral stimuli report that only one M-cell is active at a time [S4, S5, S7]. In contrast, we observe concurrent activity in the M-cells (Figure S4D). This is consistent with a study by Satou and colleagues [S6] who find that the M-cells were coactive 55% of the time in response to non-directional stimuli. Their data suggest that in these cases, both M-cells fire, but with a delay, and that the excitatory effects of the trailing spikes are shunted by commissural inhibitory neurons in the spinal cord. However, the authors observe a higher probability of co-activity in the M-cells by calcium imaging compared to what was inferred from behavioral analysis (55% vs. 30%). Therefore, the calcium transients observed may not be accurate predictors of action potentials. Instead, they may primarily reflect sensory input rather than output. It is conceivable that the strong excitatory drive generated by auditory/vestibular afferents can saturate the slow-kinetic calcium indicator in the M-cell soma, and mask the potential effect of backpropagating depolarization. In our ablation experiments, direct sensory input is intact and may dominate measurable somatic calcium entry in the M-cell. Thus, our results imply that dendritic afferents elicit the bulk of calcium entry into the M-cell soma and that spiral fiber neuron actions are primarily restricted to the axon hillock. Since M-cell mediated behavior is impaired in the absence of spiral fiber neurons, it suggests spiral fiber neuron and dendritic inputs are integrated not in the M-cell soma but rather at the level of the M-cell axon hillock, the site of action potential initiation [S8].

## SUPPLEMENTAL EXPERIMENTAL PROCEDURES

### Zebrafish care and strains

All protocols and procedures involving zebrafish were approved by the Harvard University/Faculty of Arts & Sciences Standing Committee on the Use of Animals in Research and Teaching (IACUC). Larvae were raised at 28.5°C on a standard 14/10 hour light/dark cycle at a density of 20-50 fish in 10 cm diameter petri dishes filled with 25-40 mL buffered E3 (1mM HEPES added). *Mitfa-/-* mutants that lack melanophores were used for all ablation and calcium imaging experiments.

### Generation of transgenic fish

*Tg(-6.7FRhcrtR:gal4VP16)*: -6.7FRhcrtR was amplified using a nested PCR strategy. First, a 6775bp DNA fragment immediately upstream of the *Fugu rubripes hcrtr2* start site was amplified from genomic DNA, using a high-fidelity polymerase (PfuUltra II Fusion, Stratagene) with primers 5'-AATCCAAATTCCCAGTGACG-3' and 5'- CCAGATACTCGGCAAACAAA-3', 56° C annealing temperature, 1:45 elongation time. The PCR product was TOPO cloned into a TA vector (Life Technologies). Using the resulting plasmid as a template, a 6732bp fragment was amplified using primers 5'- AATCCAAATTCCCAGTGACG-3' and 5'-CCAGATACTCGGCAAACAAA-3', 55°C annealing temperature, 1:45 elongation and similarly TOPO cloned into a GATEWAY-compatible vector (PCR8/GW, Life Technologies). The resulting entry vector was recombined into a destination vector upstream of gal4-VP16, between Tol2 integration arms [S9]. *Tg(UAS-E1b:Kaede)s1999t* [S10] embryos were injected at the one-cell stage with 0.5nL of 50ng/uL plasmid and 35ng/uL *Tol2 transposase* mRNA in water, and their progeny screened for fluorescence. One founder produced three fluorescent progeny; one survived. To identify transgenic fish without using a UAS reporter, potential carriers were genotyped using the following primers to generate a 592bp product spanning the upstream Tol2 arm and the start of the *Fugu* sequence: 5'- CAATCCTGCAGTGCTGAAAA-3' and 5'-TGATTCATCGTGGCACAAAT-3' 57°C annealing temperature, 0:30 elongation time.

*Tg(-6.7FRhcrtR:gal4VP16)* labels distributed cells in rhomomeres 2-7 of the hindbrain, including neurons in the tangential [S11] and medial vestibular nuclei, and other octavolateral nuclei. There are distributed cells in the spinal cord including the commissural primary ascending (CoPA) neurons. Dispersed cells are visible in the anterior and posterior lateral line, statoacoustic and trigeminal ganglia. In the hypothalamus, the line labels a cluster of cells that

do not overlap with oxytocin, hypocretin or QRFP positive cells. Sparse labeling is detected in the habenula and midbrain tegmentum. Skin and notochord cells are also labeled. See Movie S1.

*Tg(14xUAS-E1b:hChR2(H134R)-EYFP)*: hChR2(H134R)-EYFP [S12] was subcloned downstream of 14 copies of a UAS element and an E1b minimal promoter in a vector containing an SV40 polyA sequence and Tol2 recognition arms [S9]. This vector was co-injected with *tol2 transposase* mRNA into TLAB embryos at the single cell stage. Potential founders were screened by crossing to *Tg(isl1:Gal4-VP16,14xUAS:Kaede)* [S13] and monitoring tail movements in response to blue light from an arc lamp on a stereomicroscope (Leica MZ16) at 30 hours post-fertilization.

*Tg(UAS:GCaMP5)* was generated by LR recombination of a 14xUAS fragment upstream of *GCaMP5G* and between Tol2 recognition arms, using custom Gateway-compatible entry and destination vectors (Life Technologies). 30 ng/uL of this vector was injected with Tol2 RNA into WIK embryos at the one-cell stage. Potential founders were screened by crossing to *Tg(-6.7FRhcrtR:gal4VP16)*.

The following transgenic lines were used: *Tg(UAS-E1b:Kaede)s1999t* [S10], *Tg(UAS:GCaMP-HS)* [S14], and *Et(fos:Gal4-VP16)s1181t* [S15].

**Monitoring neural activity by calcium imaging**

Calcium imaging was performed with a custom two-photon microscope equipped with a 0.95 NA 20X (Olympus) controlled by custom software written in C# (Microsoft). Z drift was actively compensated by comparing each scanned image to an anatomical reference stack collected immediately prior to imaging. Each newly scanned image was cross correlated in three dimensions with the reference stack using Intel Performance Primitives (IPP) and C#. The lateral search size was ±10 μm and the axial search size was ±5 μm (11 image slices of the reference stack). The depth of the best z slice was low pass filtered and kept within 1 μm of the original focal plane by adjusting the objective height in 1 μm increments. Images were acquired at either 4 or 8 frames a second.

For imaging, 5-6 days post-fertilization (dpf) larvae were paralyzed by soaking in a ~50 μL droplet of 125 mM alpha-bungarotoxin (VWR, 89138-082) for 2 minutes. Fish were then rinsed in E3 and embedded in 2% low-melting point agarose (AquaPor LM, EC-204, National Diagnostics) in E3 for imaging. Neurons were labeled with the genetically-encoded calcium

indicators GCaMP-HS (*Tg(UAS:GCaMP-HS*)) for experiments described in Figures 1 and S1 and with GCaMP5 (*Tg(UAS:GCaMP5*)) for experiments in Figure S4.

Three different types of stimuli were used. Water puffs were delivered through a pipette (either a custom pulled glass pipette of ~0.3 mm inner diameter (IB120F-4, World Precision Instrument) or a blunt tip needle 25G 1½" (Jorgensen Laboratories) delivered ~0.5 mm away from the otic vesicle or the middle of the tail, where a small area was freed of agarose. The strength of the pulse varied from 10 to 40 PSI, with 5-15 ms duration, and was adjusted to obtain a high probability of reliable response without damaging the tissue. Tap stimuli were delivered to the dish holding the larva via a push type solenoid (28-I-12D, Allied Electronics) working with a spring system. The tap produced both a sound and a vibration of the water surrounding the fish. Fish whose probability of response was low or sharply decreased as the experiment progressed were excluded from the analysis (~15%).

Analysis of calcium signals was done in MATLAB (Mathworks, Natick MA). Individual images were first registered in x-y with reference to the first image of an experiment. Regions of interest (ROIs) corresponding to individual neurons or the axon cap were manually drawn. Calcium imaging data is reported as $\Delta f/f$ = (fluorescence over a selected ROI - baseline fluorescence of ROI) / (baseline fluorescence - background fluorescence). Trials for which an ROI showed activity above baseline after the stimulus were scored automatically by the analysis code as response trials and then manually verified.

For experiments combining calcium imaging in the M-cell with laser ablations of spiral fiber neurons, larvae were sequentially stimulated with taps of weak and strong intensity. The difference in magnitude with respect to sound and vibration was not precisely measured. Results were similar with taps of weak and strong intensity. To match the behavior experiments, only results with strong taps are shown. Larvae were paralyzed with alpha-bungarotoxin (Figure S4 A-D). To ensure that the toxin did not influence our experimental outcomes, non-paralyzed fish were also tested (Figure S4 E). No differences in calcium dynamics were observed, and the outcome of the ablations was similar. Post imaging was done starting 10-20 minutes after ablations. Pilot experiments indicated that there was no difference in our results if this interval was prolonged.

**High-speed behavioral analysis**

A custom-built high-speed video tracking apparatus and custom software written in C# was used to monitor and quantify escape responses to tap stimuli. It consisted of a camera (Pike F-032, Allied Vision Technologies) and variable lens (1:3.9 75 mm, 25.5 mm, Tamron) run at 1000 frames/second by binning pixels, resulting in 104 x 56 images. Larval zebrafish tails were illuminated with IR light. In a manner similar to the calcium imaging experiments, the software sent voltage pulses to a solenoid fixed to the dish holder on which the larva was placed. Different voltages were used to produce taps of three different intensities: small, medium, and strong, which were empirically determined. Because different voltages gave rise to varying stimulus timing, actual tap timing was monitored using a small piezo element (Sparkfun Electronics SEN-10293) mounted close to the solenoid. As recorded by the piezo element, vibration of the dish lasted on the order of 100 ms. A stimulus interval of 20 seconds was used, with which no habituation was observed. Due to the non-directional nature of the stimulus, escapes occurred in either direction. The software tracked tail position online using five equidistant points positioned on the tail. Analysis of tail segment angles was done offline with custom-written scripts in MATLAB. Tail angles reported correspond to the angle of the last tail segment with respect to the vertical. Response latency was defined as the interval between the tap and the first frame at which a tail movement was detected. Tail traces were smoothed using a Butterworth filter ($4^{th}$ order, cutoff = 0.15 Hz). Scripts automatically detected responses and classified them as escapes or non-escapes and detected escape latency. All classifications were then manually verified. Escapes were defined as responses beginning with a turn exceeding 60 degrees in amplitude in the first 25 ms after the stimulus.

To test behavior, 5-7 dpf fish were embedded in 2% low-melting point agarose on a 35 mm diameter petri dish lid, and a scalpel was used to free the tail. A glass cover slip (Gold Seal cover glass, 48x60 mm No.1) was secured with high vacuum grease (Dow Corning) on top of the dish to make a tight water seal and prevent shadows caused by water vibrations. Larvae were allowed to acclimate for at least 30 minutes and then tested individually in the behavioral apparatus for 20 minutes in the dark. Fish were stimulated with the three alternating tap intensities. The outcome of ablations was similar across tap intensities. Only the strongest tap stimulus is shown in Figures 2 and 3 because it elicited the greatest number of escapes. Individual fish whose initial probability of fast escapes averaged over all tap intensities was below 50% were deemed unhealthy and discarded from the analysis (~10% of fish).

Homozygous *mariner* mutants [S16] deficient in hair cell mechanotransduction [S17] were screened based on their lack of a swim bladder, their lying on their side, and their circling movements in response to touch at 4 dpf. Neomycin (neomycin sulfate, Invitrogen 21810-031) treatment was used to kill lateral line neuromasts [S18]. A 50 mM stock solution in E3 was stored at 4°C and diluted 1:100 to use at a final concentration of 500 μM. Larvae were allowed to swim in this solution for 20 minutes and then washed 3 times in E3. Behavioral tests were done no later than 2 hours after treatment to avoid regeneration of neuromasts. Loss of neuromasts was verified on non-tested fish by staining with 2.6 mM DASPEI (2-(4-(dimethylamino)styryl)-N-Ethylpyridinium Iodide, Invitrogen D-426) for 20 minutes [S18].

Experiments involving neuron ablations were done in one day. Baseline responses were recorded in the morning. Larvae were subsequently anesthetized (0.016% w/v tricaine methane sulfonate, Sigma A5040) and placed under a two-photon microscope for neuronal ablations. After the ablation procedure lasting 5-20 minutes, the anesthetic solution was replaced with E3 and larvae were allowed to recover for at least 4 hours and no more than 10 hours before testing their behavior post-ablation.

**Laser ablation of neurons**

A pulsed two-photon laser was used to ablate specific cells in the M-cell circuit. Laser pulses were focused with a 0.95 NA 20X objective (Olympus) and generated from a Ti:Sapphire system (Spectra Physics MaiTai HP) operating at a 80 MHz repetition-rate with a <100 fs pulse duration. Two methods were used alternatively to achieve neuronal ablation. In one method, the laser was scanned in a spiral pattern over a small area of a selected cell with increasing power [S19]. When brief flashes of high intensity were detected by the software, scanning was automatically stopped. These flashes are thought to arise from absorption of multi-photon energy by water molecules, creating plasma and killing the cell [S20]. An alternative method consisted in sending a single high-power and brief (20-100 ms) pulse. We used a maximum power at sample of 200 mW (820 nm) measured with a power meter (Thorlabs S130C). In most cases, brief flashes of high intensity were observed at the PMT, suggesting plasma formation.

We used different indicators in neurons for ablations: UAS driving *ChR2*, *GCaMP-HS*, *GCaMP5* or *Kaede*. Neurons were targeted based on anatomy and were ablated starting with the ventral-most neurons. For M-cell ablations, two locations on the soma were targeted to prevent the cell from recovering. The number of labeled spiral fiber neurons varied by fish between 6-10 cells on

each side. All labeled neurons were targeted, however, it is possible that some ablations were unsuccessful, given the tight packing of cells. Deeper spiral fiber neurons were more challenging to ablate, and sometimes required several attempts with increasing laser pulse lengths. For control ablations, we ablated neurons labeled in *Tg(-6.7FRhcrtR:gal4VP16)* with no apparent connections to the escape circuit and located 20-40 μm rostral and no more than 10 μm away dorsally or ventrally from spiral fiber neuron somata, consisting of 2-6 neurons on each side. Brains were imaged immediately and usually 24 hours after ablation to evaluate the specificity and extent of lesions.

**ChR2 stimulation**

A 473 nm diode pumped solid state blue laser (DPSSL-473-10, Roithner LaserTechnik) was used to excite ChR2 in heterozygote *Tg(-6.7FRhcrtR:gal4VP16); Tg(UAS:ChR2(H134R)-EYFP)* larvae. The laser beam was focused with a lens on the larva's head to a spot size of approximately 250 μm in diameter (see Figure 4A) with 13 mW power over the sample. 5-7 dpf larvae were embedded in agarose and their tail freed. Escape behavior was then tested in the behavioral apparatus described above, and the tap intensity was optimized for each fish in order to obtain a 5-50% probability of short-latency escapes. Approximately 30 trials were used for each of the following three conditions: 1) low-intensity taps delivered on their own, 2) the same taps paired with a 100 ms blue light pulse delivered 20-60 ms before the taps, and 3) 100 ms light pulses delivered alone. Latency was computed as the time between the onset of the tap and the first movement of the tail, or in the case of the blue light only, from the onset of the light pulse. The delay used between the light and tap in condition 2) was increased if a 20 ms delay did not result in an enhancement of short-latency escapes. For 10/22 ChR2+ larvae, the delay was 20 ms. The mean latency of escapes to blue light only across these fish was 63 ms (± 25 ms standard deviation). For 11/22 fish, the delay was 60 ms and the mean latency of escapes to blue light only across the 7 fish that responded was 92 ms ± 35 ms. One fish was tested with a 40 ms delay and produced escapes with an average latency of 72 ms. Since short-latency escapes occur within 12 ms of the tap, this implies that the escapes assigned as short-latency in condition 2) were generally not caused by the blue alone but by the combination of light and tap (see Figures 4B and S3 E, F and G). It is possible that a subset of long-latency escapes, however, are an effect of the light only stimulus, which could account for the higher probability of long-latency escapes in condition 2) (see Figure S3 A). The delays used for condition 2) in control ChR2- siblings matched in number those used for ChR2+ larvae.

Ablations of spiral fiber neurons were carried out as described above. Larvae were allowed 4-6 hours to recover from the anesthetic before testing post ablation behavior.

**Sparse neuron labeling**

To label a small number of spiral fiber neurons (Figure 1A), 0.5 nL of 30 ng/μL of plasmid encoding GFP with an N-terminal GAP43 membrane localization sequence [S11] dissolved in water was injected at the one-cell stage into *Tg(-6.7FRhcrtR:gal4VP16)* fish. Embryos were screened under a fluorescent stereoscope (Leica MZ16) with a GFP emission filter. ~10% of embryos had sparse labeling of neurons in the nervous system. The other ~90% either showed no expression or broad expression. Individual spiral fiber neurons were identified by fluorescence at 72 hours post fertilization.

**Retrograde labeling of reticulospinal neurons**

To label the reticulospinal system including the M-cells, we backfilled neurons from the spinal cord. 5 dpf larvae were anesthetized and placed on a dish filled with solidified 5% agarose. Excess water surrounding the fish was removed with a paper wipe in order to stabilize it. A scalpel was used to sever the spinal cord just caudal of the swim bladder. A sharpened tungsten needle was dipped in a drop of ~40 mM tetramethylrhodamine dextran (Life Technologies, D-3308) whose consistency was adjusted with water to make a gel-like substance. The needle was then placed onto the cut in the spinal cord. Larvae were immediately transferred to E3 and allowed to recover for two hours, while the die filled the reticulospinal system. Their brains were then imaged with a Zeiss LSM 780 NLO microscope used as a confocal.

**Immunohistochemistry**

For Movie S1, 6 dpf *Tg(-6.7FRhcrtR:gal4VP16); Tg(UAS-E1b:Kaede)s1999t* larvae were fixed in 4% PFA in PBT (PBS + 0.25% TritonX), and stained with rabbit anti-Kaede (1:500, PM012, MBL) and mouse anti-ERK1/2 (1:500, #4696, Cell Signaling), and alexa-congugated secondary antibodies (1:500, goat anti-mouse IgG Alexa Fluor® 647, A-21235 and goat anti-rabbit IgG Alexa Fluor® 546, A-11035, Life Technologies). Fish were imaged by confocal microscopy using a 20x 1.0 NA objective.

### Statistics

Significance was determined using the Wilcoxon signed rank test for paired data and the Wilcoxon rank sum test for independent samples. All data are reported as mean ± standard error of the mean.

## SUPPLEMENTAL REFERENCES


S1. Kimmel, C. B., Powell, S. L., and Metcalfe, W. K. (1982). Brain neurons which project to the spinal cord in young larvae of the zebrafish. J Comp Neurol *205*, 112–127.

S2. Koyama, M., Kinkhabwala, A., Satou, C., Higashijima, S.-I., and Fetcho, J. (2011). Mapping a sensory-motor network onto a structural and functional ground plan in the hindbrain. Proc Natl Acad Sci USA *108*, 1170–1175.

S3. Scott, J. W., Zottoli, S. J., Beatty, N. P., and Korn, H. (1994). Origin and function of spiral fibers projecting to the goldfish Mauthner cell. J Comp Neurol *339*, 76–90.

S4. Kohashi, T., and Oda, Y. (2008). Initiation of Mauthner- or non-Mauthner-mediated fast escape evoked by different modes of sensory input. J Neurosci *28*, 10641–10653.

S5. O'Malley, D. M., Kao, Y.-H., and Fetcho, J. R. (1996). Imaging the functional organization of zebrafish hindbrain segments during escape behaviors. Neuron *17*, 1145–1155.

S6. Satou, C., Kimura, Y., Kohashi, T., Horikawa, K., Takeda, H., Oda, Y., and Higashijima, S.-I. (2009). Functional role of a specialized class of spinal commissural inhibitory neurons during fast escapes in zebrafish. J Neurosci *29*, 6780–6793.

S7. Kohashi, T., Nakata, N., and Oda, Y. (2012). Effective Sensory Modality Activating an Escape Triggering Neuron Switches during Early Development in Zebrafish. J Neurosci *32*, 5810–5820.

S8. Furshpan, E. J., and Furukawa, T. (1962). Intracellular and extracellular responses of the several regions of the Mauthner cell of the goldfish. J Neurophysiol *25*, 732–771.

S9. Urasaki, A., Morvan, G., and Kawakami, K. (2006). Functional dissection of the Tol2 transposable element identified the minimal cis-sequence and a highly repetitive sequence in the subterminal region essential for transposition. Genetics *174*, 639–649.

S10. Scott, E. K., Mason, L., Arrenberg, A. B., Ziv, L., Gosse, N. J., Xiao, T., Chi, N. C., Asakawa, K., Kawakami, K., and Baier, H. (2007). Targeting neural circuitry in zebrafish using GAL4 enhancer trapping. Nat Methods *4*, 323–326.

S11. Bianco, I. H., Ma, L.-H., Schoppik, D., Robson, D. N., Orger, M. B., Beck, J. C., Li, J. M.,

Schier, A. F., Engert, F., and Baker, R. (2012). The tangential nucleus controls a gravito-inertial vestibulo-ocular reflex. Curr Biol *22*, 1285–1295.

S12. Zhang, F., Wang, L.-P., Brauner, M., Liewald, J. F., Kay, K., Watzke, N., Wood, P. G., Bamberg, E., Nagel, G., Gottschalk, A., et al. (2007). Multimodal fast optical interrogation of neural circuitry. Nature *446*, 633–639.

S13. Pan, Y. A., Choy, M., Prober, D. A., and Schier, A. F. (2012). Robo2 determines subtype-specific axonal projections of trigeminal sensory neurons. Development *139*, 591–600.

S14. Muto, A., Ohkura, M., Kotani, T., Higashijima, S.-I., Nakai, J., and Kawakami, K. (2011). Genetic visualization with an improved GCaMP calcium indicator reveals spatiotemporal activation of the spinal motor neurons in zebrafish. Proc Natl Acad Sci USA *108*, 5425–5430.

S15. Scott, E. K., and Baier, H. (2009). The cellular architecture of the larval zebrafish tectum, as revealed by gal4 enhancer trap lines. Front. Neural Circuits *3*, 13.

S16. Nicolson, T., Rüsch, A., Friedrich, R. W., Granato, M., Ruppersberg, J. P., and Nüsslein-Volhard, C. (1998). Genetic analysis of vertebrate sensory hair cell mechanosensation: the zebrafish circler mutants. Neuron *20*, 271–283.

S17. Ernest, S., Rauch, G. J., Haffter, P., Geisler, R., Petit, C., and Nicolson, T. (2000). Mariner is defective in myosin VIIA: a zebrafish model for human hereditary deafness. Hum. Mol. Genet. *9*, 2189–2196.

S18. Harris, J. A., Cheng, A. G., Cunningham, L. L., MacDonald, G., Raible, D. W., and Rubel, E. W. (2003). Neomycin-Induced Hair Cell Death and Rapid Regeneration in the Lateral Line of Zebrafish (Danio rerio). JARO - Journal of the Association for Research in Otolaryngology *4*, 219–234.

S19. Orger, M. B., Kampff, A. R., Severi, K. E., Bollmann, J. H., and Engert, F. (2008). Control of visually guided behavior by distinct populations of spinal projection neurons. Nat Neurosci *11*, 327–333.

S20. Vogel, A., and Venugopalan, V. (2003). Mechanisms of pulsed laser ablation of biological tissues. Chem. Rev. *103*, 577–644.